

Differentiable Maximum Likelihood Noise Estimation for Quantum Error Correction

Hanyan Cao,^{1,*} Dongyang Feng,^{2,*} Cheng Ye,^{2,3} and Feng Pan^{1,†}

¹*Science, Mathematics and Technology Cluster, Singapore University of Technology and Design, 8 Somapah Road, 487372 Singapore*

²*CAS Key Laboratory for Theoretical Physics, Institute of Theoretical Physics, Chinese Academy of Sciences, Beijing 100190, China.*

³*School of Physical Sciences, University of Chinese Academy of Sciences, Beijing 100049, China*

Accurate noise estimation is essential for fault-tolerant quantum computing, as decoding performance depends critically on the fidelity of the circuit-level noise parameters. In this work, we introduce a differentiable Maximum Likelihood Estimation (dMLE) framework that enables exact, efficient, and fully differentiable computation of syndrome log-likelihoods, allowing circuit-level noise parameters to be optimized directly via gradient descent. Leveraging the exact *Planar* solver for repetition codes and a novel, simplified Tensor Network (TN) architecture combined with optimized contraction path finding for surface codes, our method achieves tractable and fully differentiable likelihood evaluation even for distance 5 surface codes with up to 25 rounds. Our method recovers the underlying error probabilities with near-exact precision in simulations and reduces logical error rates by up to 30.6(3)% for repetition codes and 8.1(2)% for surface codes on experimental data from Google’s processor compared to previous state-of-the-art methods: correlation analysis and Reinforcement Learning (RL) methods. Our approach yields provably optimal, decoder-independent error priors by directly maximizing the syndrome likelihood, offering a powerful noise estimation and control tool for unlocking the full potential of current and future error-corrected quantum processors.

Fault-tolerant quantum computing (FTQC) promises to unlock computational capabilities far beyond classical reach, from simulating many-body quantum systems to solving industrially relevant optimization problems [1–3]. Realizing this promise hinges on quantum error correction (QEC), which protects fragile logical information by encoding it redundantly across many physical qubits and continuously measuring error syndromes [4, 5]. The effectiveness of QEC, however, is only as good as the decoder that interprets these syndromes—and the decoder, in turn, is only as good as the noise model it assumes [6]. In practice, the noise affecting a quantum processor is described by a detector error model (DEM) that assigns prior probabilities to each possible error mechanism in the circuit [7, 8]. When these priors deviate from the true physical noise, decoding quality deteriorates sharply: Google’s landmark surface code experiment demonstrated that accurately estimated circuit-level noise parameters were essential to achieving below-threshold error suppression [5], and subsequent studies have shown that even modest prior inaccuracies can erode the exponential suppression expected from increasing code distance [9]. Accurately estimating DEM priors from experimental data is therefore the central bottleneck standing between today’s noisy hardware and the full error-suppression power of QEC.

The challenge of noise estimation lies in the inverse nature of the problem: physical errors are not directly observable; only their degenerate mappings, syndromes, are measured. Consequently, the task is to infer the underlying error probabilities that maximize the likelihood

of the observed syndrome statistics. While this is fundamentally a parameter estimation problem, the high-dimensional space of error configurations makes direct inference computationally intractable for general codes.

Previous efforts to address this challenge have primarily focused on correlation analysis and machine learning approaches. Methods based on syndrome correlations [10] have been widely adopted; for instance, Google utilized correlation analysis to characterize noise in their repetition code [4] and surface code [5] experiments. More recently, Remm *et al.* demonstrated experimentally informed decoding by refining noise models via correlations [11]. Several other works have extended syndrome-statistics-based DEM estimation to broader settings, including systematic parameter recovery from syndrome data [12, 13], application to more sophisticated experimental data [14], and adaptive tracking of drifting noise [15]. While valuable, these correlation-based methods estimate error rates from local syndrome statistics but do not directly optimize a global likelihood objective over the full joint distribution of detection events. Moreover, correlation analysis is fundamentally limited to pairwise error interactions and cannot be straightforwardly applied to codes with higher-order correlations, such as color codes—indeed, Google’s recent color code experiment on Willow had to forgo correlation-derived DEMs entirely [16]. Even for surface codes, correlation analysis can produce unphysical error probabilities (including negative values) that cause decoders to fail [9]. Alternatively, reinforcement learning (RL) has been proposed to optimize decoder priors by treating the logical error rate as a reward signal, bypassing the need for explicit noise modeling [9, 17]. Although RL agents can adapt to complex noise environments, the optimized parameters lack direct correspondence to in-

* These authors contributed equally to this work.

† feng_pan@sutd.edu.sg

dividual physical error mechanisms, making it difficult to extract meaningful noise diagnostics from the learned model. Moreover, RL performance depends critically on a good initialization, typically provided by correlation analysis, thereby inheriting and being bounded by the same limitations of the underlying correlation-based estimates [9]. Furthermore, as we demonstrate in this work, RL-optimized priors are inherently coupled to the specific decoder employed during training, exhibiting significantly degraded performance when transferred to other decoding algorithms. An additional practical limitation is that RL requires executing a decoder in the inner loop to evaluate rewards, restricting its use to fast but sub-optimal decoders and precluding optimization toward the higher-fidelity decoding strategies.

In this Letter, we propose a rigorous, physics-inspired framework to estimate the DEM prior using differentiable Maximum Likelihood Estimation (dMLE). Our approach leverages the insight that calculating the likelihood of a syndrome is mathematically equivalent to computing the partition function of a statistical mechanical spin model. By utilizing the exact planar solver developed by Cao *et al.* [18] for repetition codes and employing Tensor Networks (TNs) for surface codes, we can compute these likelihoods efficiently and exactly. This formulation allows us to optimize error probabilities directly via gradient-based backpropagation. Rather than relying on heuristic or RL-based methods, our approach directly estimates the probability of each individual error mechanism, yielding a noise model whose parameters carry clear physical meaning and explicitly minimize the mismatch between the estimated and true error distributions. We validate our method on both simulated and experimental data, achieving logical error rate reductions of up to 30.6(3)% for repetition codes and 8.1(2)% for surface codes, and demonstrating superior generalizability across all tested decoders compared to both correlation-analysis and RL-based approaches.

Maximum Likelihood Noise Estimation.— In circuit-level noise scenarios, conventional Pauli error models on qubits often fail to capture the intricate dynamics of fault-tolerant protocols. To address this, researchers employ the Detector Error Model (DEM), which characterizes the probabilistic relationships between error mechanisms and detectors (combinations of syndromes) within a spacetime circuit. A DEM is formally represented as a hypergraph: nodes correspond to detectors, while hyperedges denote independent error mechanisms that trigger specific sets of detectors [8]. This abstraction is particularly advantageous for decoding, as it provides a direct mapping from physical errors to the observed syndrome history.

In this framework, we consider that the underlying noise process is decomposed into n independent error mechanisms $\{e_i, i = 0, 1, \dots, n\}$, each occurring with a probability θ_i , and $\mathbf{e} \in \{0, 1\}^n$ represents an error configuration. The collection of these probabilities $\boldsymbol{\theta} = \{\theta_i\}$ constitutes the prior parameters of the de-

tector error model. Our goal is to estimate $\boldsymbol{\theta}$ from a dataset of observed detection events $\{\mathbf{s}^{(1)}, \mathbf{s}^{(2)}, \dots, \mathbf{s}^{(N)}\}$ with $\mathbf{s} \in \{0, 1\}^m$, where m is the number of detectors.

The probability of observing a specific detection event \mathbf{s} given the model parameters $\boldsymbol{\theta}$ is the sum of the probabilities of all error configurations \mathbf{e} that are consistent with \mathbf{s} :

$$p_{\boldsymbol{\theta}}(\mathbf{s}) = \sum_{\mathbf{e} \in \mathcal{C}(\mathbf{s})} p_{\boldsymbol{\theta}}(\mathbf{e}), \quad (1)$$

where $\mathcal{C}(\mathbf{s})$ denotes the set of all errors that cause the same \mathbf{s} . In the context of maximum likelihood decoding, this quantity corresponds to the summation of all logical coset probabilities — or equivalently, the summation of partition functions from a statistical mechanical perspective [19].

We formulate the estimation problem as a maximum likelihood estimation task. We seek to find the parameters $\boldsymbol{\theta}$ that maximize the log-likelihood of the observed dataset which results in a negative log likelihood (NLL) loss:

$$\mathcal{L}(\boldsymbol{\theta}) = -\mathbb{E}_{\mathbf{s} \sim p_{\text{data}}(\mathbf{s})} [\log p_{\boldsymbol{\theta}}(\mathbf{s})]. \quad (2)$$

To optimize this loss function, we employ gradient descent to update parameters until the loss converges. However, the primary challenge lies in the efficient computation of $p_{\boldsymbol{\theta}}(\mathbf{s})$ and its gradients. As defined in Eq. (1), this requires a summation over all equivalent error configurations. By mapping the DEM to a statistical physics model, this summation is shown to be equivalent to calculating the partition function of a corresponding spin system—a task that is generally #P-complete [18–20]. However, the *Planar* method proposed by Cao *et al.* [18] demonstrates that for the planar cases, this problem is solvable in polynomial time using the Kac-Ward solution. For example, the DEMs of repetition codes under circuit-level noise are typically planar. Consequently, the distribution $p_{\boldsymbol{\theta}}(\mathbf{s})$ becomes tractable for repetition codes by summing all dual variables as illustrated in Fig. 1 (a). For a given \mathbf{s} , we first identify a pure error \mathbf{e} that satisfies this constraint. This step can be efficiently solved in parallel via Gaussian Elimination. We then construct a dual spin model with couplings $J_i = (-1)^{e_i} \frac{1}{2} \log \frac{1-\theta_i}{\theta_i}$ where the signs of couplings are determined by non-trivial action of the pure error on the i th qubit. Finally, an auxiliary spin is introduced to restore the complete planarity of the graph, allowing the partition function \mathcal{Z} to be efficiently calculated using Kac-Ward determinant formula [21].

Surface codes, characterized by a significantly more complex decoding structure, cannot be handled directly by the *Planar* method. We therefore employ Tensor Networks (TNs) to facilitate the surface code optimization. In the TN framework, the calculation of probabilities is achieved more directly. Eq. (1) can be rewritten in the following equivalent form:

$$p_{\boldsymbol{\theta}}(\mathbf{s}) = \sum_{\mathbf{e}} p(\mathbf{e}) \cdot \delta_{\mathbf{s}, \mathbf{s}_{\mathbf{e}}}, \quad (3)$$

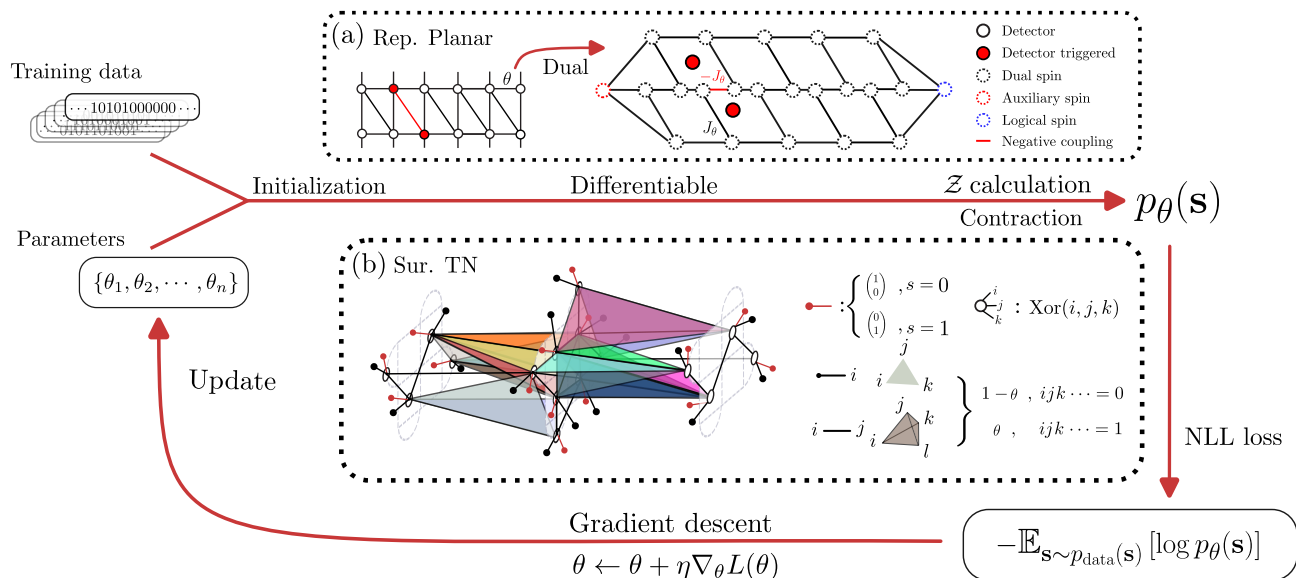


FIG. 1. **Differentiable Maximum Likelihood Noise Estimation (dMLE) Framework.** (1) Initialization: Observed detection events \mathbf{s} and parameters θ are mapped to dual spin models (Repetition codes) or Tensor Networks (Surface codes). (2) Evaluation: The NLL loss is derived from the partition function \mathcal{Z} or TN contraction. (3) Update: Since all of the above processes are differentiable, parameters are iteratively refined via gradient descent until convergence to the maximum likelihood estimate. (a) DEM of $d = 3$, $r = 5$ repetition code memory circuit and dual spin glass model. The white (red) nodes are detectors (triggered) and the black edges are error mechanisms. Each black dashed node is a dual spin. The blue dashed node is the logical spin, whose ∓ 1 configurations represent whether a logical error occurs. The red dashed node is an auxiliary spin, which is added to reconstruct the planarity. (b) Tensor Network of $d = 3$ and $r = 2$ surface code. White nodes are XOR tensors, which enforce detector parity, with red dangling edges imposing detection constraints. Probability tensors (black edges, colored surfaces/bodies) encode error mechanisms, assigning weights θ_i and $1 - \theta_i$ to triggered and non-triggered states, respectively.

where the summation runs over all possible error configurations, and the Kronecker delta $\delta_{\mathbf{s}, \mathbf{s}_e}$ ensures that only errors consistent with the observed \mathbf{s} contribute to the total probability. This product-sum form is particularly well-suited for representation as a Tensor Network [5, 22–24].

Fig. 1 (b) illustrates the TN for distance-3 and round-2 surface code Z -basis memory experiment. In this representation, each detector is represented by an XOR tensor, which enforces even parity across all its connected legs. Each detection event constraint is incorporated via a red dangling edge on the XOR tensor, which restricts the error configuration space by half. The black edges, colored surface and bodies represent probability tensors which contain only two non-zero elements θ_i and $1 - \theta_i$ corresponding to whether the i th error mechanism is triggered or not respectively. Consequently, contracting the TN constructed through this process yields the exact probability $p_\theta(\mathbf{s})$ for the given \mathbf{s} .

Both the *Planar* and TN summation methods are fully differentiable with respect to their input parameters, enabling gradient-based optimization to determine the maximum likelihood estimation of the noise parameters. As depicted in Fig. 1, the training process begins by mapping the observed detection events \mathbf{s} and the initial parameters θ onto either a dual spin model or a TN. The partition function \mathcal{Z} of the dual spin model or the TN

contraction then yields the parameterized probabilities and the NLL loss. The parameters are iteratively refined through the update rule $\theta \leftarrow \theta + \eta \nabla_\theta \mathcal{L}(\theta)$, where η denotes the learning rate. Once the loss function converges, the resulting θ yields the maximum likelihood estimate that best characterizes the noise distribution of the dataset.

Numerical Results.— To demonstrate the efficacy of our dMLE method, we conducted numerical experiments focusing on two key aspects: the accuracy of the recovered error parameters and the subsequent suppression in logical error rates.

We first tested the capability of our method via numerical simulations on a repetition code instance with $d(\text{distance}) = 7$ and $r(\text{round}) = 7$. We employed standard Monte Carlo gradients to approximately optimize the loss function—a technique common in machine learning contexts. The results are visualized in Fig. 2 (upper). The orange dashed line also represents the initialization, which exhibits significant fluctuations and deviates from the real values (black line). The blue, purple, and red dots correspond to different stages of the optimization results. As shown in the main plot, the optimized prior probabilities progressively converge toward the true values during training, with the final optimized parameters (red dots) showing excellent agreement with the true values. Additionally, the inset quantitatively illustrates the

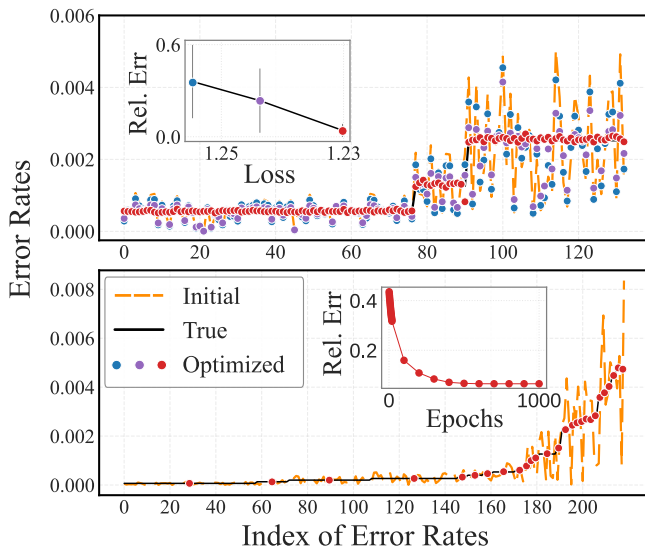


FIG. 2. (Upper) Optimization dynamics for a $d = 7$ and $r = 7$ repetition code. The orange dashed line represents the noisy initialization, while black lines denote the ground truth. Colored dots (blue to red) indicate parameter evolution during training, with final red dots showing excellent agreement with the true values. Inset: Correlation between the optimization objective (NLL loss) and parameter accuracy (relative error), demonstrating that minimizing approximate NLL directly improves estimation fidelity. (Lower) Surface code reconstruction ($d = 3$, $r = 5$, $\epsilon_p = 0.001$). Comparison of initial (orange dashed), optimized (red dots), and true (black lines) parameters for a rotated surface code using Tensor Network contraction. For visual clarity, the red dots in the main plot represent the mean results obtained by grouping different optimized priors with the same ground truth value. The method effectively recovers the underlying detector error models.

relation between the optimization objective and parameter accuracy. By plotting the Relative Error against the Loss, we demonstrate that minimizing the approximate NLL via Monte Carlo gradients directly drives a reduction in the relative error of the estimated priors.

We then assessed the performance of our optimization scheme on surface codes. The complexity of the DEM for surface codes renders the *Planar* method inapplicable, instead, Tensor Networks (TNs) are employed to compute the summation in Eq. (1). We simulated a $d = 3$ and $r = 5$ rotated surface code Z-basis memory experiment with a depolarizing error rate of $\epsilon_p = 0.001$ using Stim [7]. The optimization results are presented in Fig. 2 (lower). We applied the same random perturbation scheme to deviate the initial parameters (orange dashed line) from the true values (black line). As training converges, the optimized parameters (red dots) are also effectively congruent with the analytical optima.

These simulation results for both repetition and surface codes confirm that our method effectively reconstructs the underlying physical error model, and that Monte Carlo gradients remain robust even for large systems where the exact NLL loss is intractable.

Having validated our method on simulated scenario, we extended our investigation to experimental data to assess performance under real-world conditions. In this case, the underlying true prior distributions are unknown; consequently, the logical error rate constitutes a robust metric for evaluating optimization performance.

We first utilized repetition code data from the superconducting platform at the Beijing Academy of Quantum Information Sciences (BAQIS) [18]. Fig. 3 (left) presents the logical error probability per round P_L as a function of code distance $d \in \{3, 5, 7, 9\}$. The dashed lines represent the performance using the initial parameters (from correlation analysis [4]), while the solid lines correspond to the results after optimization. As illustrated, our method consistently reduces the logical error rates for both the Minimum Weight Perfect Matching (MWPM) [25, 26] and *Planar* decoders across all distances. This signifies that the optimized prior distribution aligns more closely with the physical reality of the noise.

Notably, the optimization yields a more pronounced gain for the *Planar* decoder, as indicated by the larger shaded region between the initial and optimized curves compared to MWPM. This observation is quantitatively supported by the inset, which details the relative improvement percentage. While the MWPM decoder shows a modest improvement up to 8.6(6)%, the *Planar* decoder achieves a substantial performance boost, with improvements reaching up to 30.6(3)% at larger distance. These results confirm that our gradient-based optimization can effectively extract more accurate noise information from experimental data, thereby enhancing the decoder’s error suppression capability.

Finally, we analyzed $d = 5$ surface code experimental data from Google’s Sycamore processor [27], which includes 5 to 25 QEC rounds. A central enabler of this analysis is our novel tensor network architecture for the DEM likelihood computation: by applying a Walsh-Hadamard decomposition of XOR tensors, we dramatically simplify the network topology, reducing it to only Hadamard matrices and one-dimensional probability vectors. Combined with state-of-the-art contraction path optimization [28–31], the resulting contraction complexity of TN for $d=5$ surface codes remains manageable across all round numbers for both optimization and decoding tasks—in stark contrast to the previous estimate of tens of CPU years under the boundary MPS scheme [32] (for more details about the TN structure, complexity analysis and TN decoding tasks, please refer to the Supplementary Material [33]). Moreover, the entire contraction pipeline is fully differentiable [34], enabling end-to-end gradient-based optimization of the DEM parameters. For training efficiency, we optimized on 5-round data and broadcasted the learned parameters of repeated cycles to larger round numbers, a standard strategy that leverages time-translation symmetry in quantum memory experiments [9, 35]; in principle, our framework also supports joint optimization across all rounds simultaneously.

Without losing generality, we set the SI1000 DEM [36]

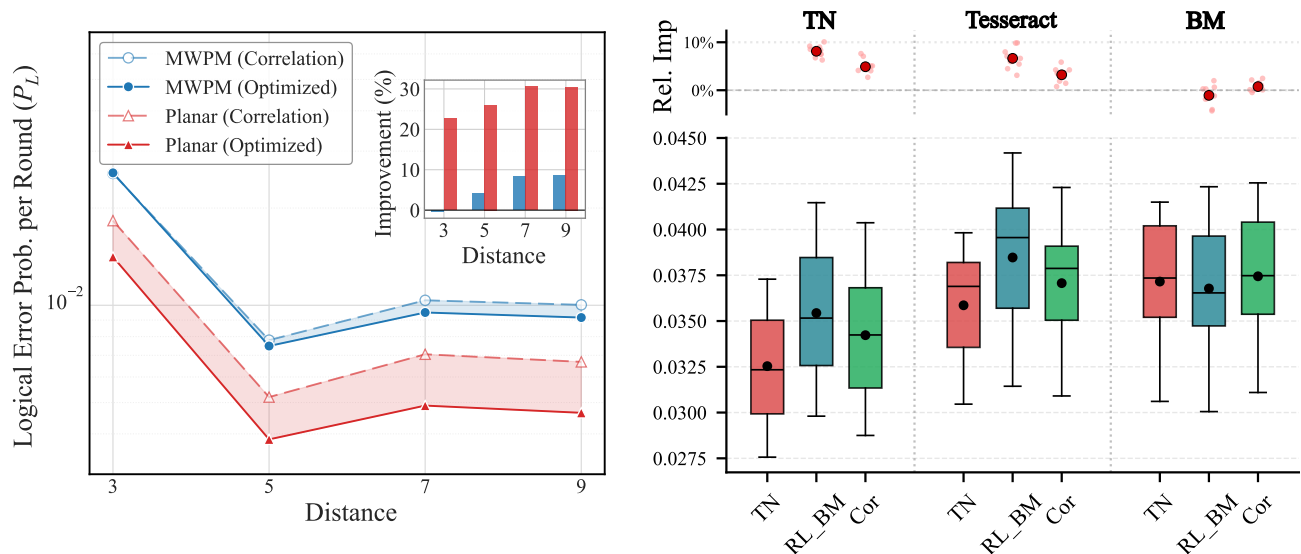


FIG. 3. Numerical Results. (left) Experimental validation on BAQIS superconducting repetition codes. Logical error probability per round P_L versus code distance $d \in \{3, 5, 7, 9\}$. Dashed lines correspond to initial parameters derived from correlation analysis, while solid lines represent performance after our optimization. The method consistently suppresses errors for both MWPM and *Planar* decoders. Inset: Relative improvement percentages, highlighting a significant gain for the *Planar* decoder at larger distances. (right) Optimization on Google Sycamore surface code ($d = 5$) dataset. Logical error rates compared across three decoders (TN, Tesseract, Belief Matching) using DEMs derived from three distinct sources: our TN-based optimization, RL-based Belief Matching, and correlation analysis. Our TN-optimized DEM demonstrates superior transferability, achieving the lowest logical error rates for high-performance decoders (TN and Tesseract), whereas RL-optimized models show limited generalizability outside their training decoder.

provided by Google’s dataset as the initial point for optimization. After training, we compared the performance of TN, Tesseract [37], and Belief Matching decoders [38] across three types of DEMs: those optimized by TN (ours), Belief Matching based RL which gives the lowest logical error rate in [9], and the correlation analysis in Fig. 3 (right). These results indicate that for the TN decoder, our optimized DEM reduces the logical error rate by an average of 8.1(2)% and 4.9(0)% compared to RL and correlation-based DEMs, respectively. For Tesseract, these reductions are 6.6(4)% and 3.2(1)%. In contrast, for Belief Matching, our method shows only a marginal improvement over correlation and no gain over RL. This discrepancy suggests that matching-based decoders often yield sub-optimal solutions; however, when employing a superior minimum-weight decoder like Tesseract, the maximum-likelihood-estimated DEM consistently achieves the lowest logical error rate. On the other hand, these results highlight a significant drawback of the RL-based optimization scheme: the resulting DEMs often lack generalizability, as they tend to be overfitted to the specific decoder used during training (a detailed comparison and analysis of the DEM parameters after optimization can be found in Supplementary Material [33]).

Conclusion.— In this work, we have shown that the problem of noise estimation in quantum error correction can be cast as a maximum likelihood inference task, where syndrome log-likelihoods are computed ex-

actly via statistical mechanical mappings and tensor network methods. This physics-motivated formulation provides a principled, decoder-agnostic route to learning circuit-level error parameters directly from experimental syndrome data. Our optimized priors consistently outperform both correlation-analysis and RL-based alternatives, reducing logical error rates by up to 30.6(3)% for repetition codes and 8.1(2)% for surface codes, and crucially, these gains share across all tested decoders—Planar, TN, Matching-based decoders, and Tesseract—without retraining. Furthermore, employing the highest-fidelity Tensor Network (TN) decoder in conjunction with the optimal DEM yielded an average 11.5(3)% performance improvement compare to former state-of-the-art RL-optimized Belief-Matching.

While our current exact validation on surface codes is limited to distance $d = 5$ due to computational resource constraints, the framework possesses significant potential for scalability. By leveraging the spatial translation symmetry inherent in surface codes and incorporating subsampling strategies [9, 35], our method can be effectively generalized to characterize noise in larger code distances without prohibitive costs. Furthermore, the utility of our optimized DEM extends beyond enhancing standard decoders; it provides a rigorous source of experimentally aligned training data. This is particularly crucial for empowering neural-network-based decoders [39–43], bridging the simulation-experiment gap by supplying high-fidelity samples that reflect physical noise reali-

ties. In future work, we will explore efficient approximation schemes for likelihood estimation to reduce computational overhead and broaden applicability to larger code distances. Moreover, since our framework is inherently differentiable, it can be naturally extended to estimate noise at the gate level or even the pulse level [17], potentially enabling noise-aware control optimization where physical control parameters are jointly tuned with error correction performance.

Acknowledgements.— The authors would like to thank Haifeng Yu and Huikai Xu for providing access to their experimental data, and Pan Zhang, Zixuan Lu and Zhiheng Zhang for helpful discussions. This work is supported by the Ministry of Education Singapore under grant No. SKI 2021_07_03, National Quantum Computing Hub translational fund No. W24Q3D0002 and MTC Young Individual Research Grant No. M25N8c0120.

The Python implementation of our algorithm is available at [44].

-
- [1] P. W. Shor, Scheme for reducing decoherence in quantum computer memory, *Phys. Rev. A* **52**, R2493 (1995).
- [2] A. G. Fowler, M. Mariantoni, J. M. Martinis, and A. N. Cleland, Surface codes: Towards practical large-scale quantum computation, *Phys. Rev. A* **86**, 032324 (2012).
- [3] B. M. Terhal, Quantum error correction for quantum memories, *Reviews of Modern Physics* **87**, 307 (2015).
- [4] Z. Chen, J. Kelly, C. Quintana, R. Barends, B. Campbell, Y. Chen, B. Chiaro, A. Cichy, R. Collins, W. Courtney, *et al.*, Exponential suppression of bit or phase flip errors with repetitive error correction, *Nature* **595**, 383 (2021).
- [5] R. Acharya, I. Aleiner, R. Allen, T. I. Andersen, M. Ansmann, F. Arute, K. Arya, A. Asfaw, J. Atalaya, R. Babush, *et al.*, Suppressing quantum errors by scaling a surface code logical qubit, *Nature* **614**, 676 (2023).
- [6] E. Dennis, A. Kitaev, A. Landahl, and J. Preskill, Topological quantum memory, *Journal of Mathematical Physics* **43**, 4452 (2002).
- [7] C. Gidney, Stim: a fast stabilizer circuit simulator, *Quantum* **5**, 497 (2021).
- [8] M. McEwen, D. Bacon, and C. Gidney, Relaxing hardware requirements for surface code circuits using time-dynamics, *Quantum* **7**, 1172 (2023).
- [9] V. Sivak, M. Newman, and P. Klimov, Optimization of decoder priors for accurate quantum error correction, *Phys. Rev. Lett.* **133**, 150603 (2024).
- [10] S. T. Spitz, B. Tarasinski, C. W. J. Beenakker, and T. E. O’Brien, Adaptive weight estimator for quantum error correction, *Quantum* **2**, 81 (2018).
- [11] A. Remm, N. Lacroix, L. Bödeker, E. Genois, C. Hellings, F. m. c. Swiadek, G. J. Norris, C. Eichler, A. Blais, M. Müller, S. Krinner, and A. Wallraff, Experimentally informed decoding of stabilizer codes based on syndrome correlations, *Phys. Rev. Res.* **8**, 013044 (2026).
- [12] R. Blume-Kohout and K. Young, Estimating detector error models from syndrome data, arXiv preprint arXiv:2504.14643 [10.48550/arXiv.2504.14643](https://arxiv.org/abs/10.48550/arXiv.2504.14643) (2025).
- [13] E. Takou and K. R. Brown, Estimating decoding graphs and hypergraphs of memory quantum error-correction experiments, *Phys. Rev. A* **112**, 052414 (2025).
- [14] K. E. Arms, M. J. McHugh, J. E. Nyhan, W. F. Reus, and J. L. Ulrich, Estimating detector error models on Google’s Willow (2025), [arXiv:2512.10814](https://arxiv.org/abs/2512.10814) [quant-ph].
- [15] D. Bhardwaj, E. Takou, Y. Lin, and K. R. Brown, Adaptive estimation of drifting noise in quantum error correction (2025), [arXiv:2511.09491](https://arxiv.org/abs/2511.09491) [quant-ph].
- [16] N. Lacroix, A. Bourassa, F. J. Heras, L. M. Zhang, J. Bausch, A. W. Senior, T. Edlich, N. Shutty, V. Sivak, A. Bengtsson, *et al.*, Scaling and logic in the colour code on a superconducting quantum processor, *Nature* **645**, 614 (2025).
- [17] V. V. Sivak, A. Morvan, M. Broughton, M. Neeley, A. Eickbusch, D. Abanin, A. Abbas, R. Acharya, L. A. Beni, G. Aigeldinger, *et al.*, Reinforcement learning control of quantum error correction, arXiv preprint arXiv:2511.08493 [10.48550/arXiv.2511.08493](https://arxiv.org/abs/10.48550/arXiv.2511.08493) (2025).
- [18] H. Cao, S. Zhao, D. Feng, Z. Shen, H. Yan, T. Su, W. Sun, H. Xu, F. Pan, H. Yu, and P. Zhang, Exact decoding of quantum error-correcting codes, *Physical Review Letters* **134**, 190603 (2025).
- [19] C. T. Chubb and S. T. Flammia, Statistical mechanical models for quantum codes with correlated noise, *Annales de l’Institut Henri Poincaré D* **8**, 269 (2021).
- [20] H. Bombin, R. S. Andrist, M. Ohzeki, H. G. Katzgraber, and M. A. Martin-Delgado, Strong resilience of topological codes to depolarization, *Phys. Rev. X* **2**, 021004 (2012).
- [21] M. Kac and J. C. Ward, A combinatorial solution of the two-dimensional ising model, *Physical Review* **88**, 1332 (1952).
- [22] S. Bravyi, M. Suchara, and A. Vargo, Efficient algorithms for maximum likelihood decoding in the surface code, *Phys. Rev. A* **90**, 032326 (2014).
- [23] C. T. Chubb, General tensor network decoding of 2d pauli codes (2021), [arXiv:2101.04125](https://arxiv.org/abs/2101.04125) [quant-ph].
- [24] C. Piveteau, C. T. Chubb, and J. M. Renes, Tensor-network decoding beyond 2d, *PRX Quantum* **5**, 040303 (2024).
- [25] O. Higgott, Pymatching: A python package for decoding quantum codes with minimum-weight perfect matching, *ACM Transactions on Quantum Computing* **3**, 1 (2022).
- [26] O. Higgott and C. Gidney, Sparse Blossom: correcting a million errors per core second with minimum-weight matching, *Quantum* **9**, 1600 (2025).
- [27] Google Quantum AI, [Data for ”optimization of decoder priors for accurate quantum error correction”](https://arxiv.org/abs/2404.04267) (2024).
- [28] F. Pan and P. Zhang, Simulation of Quantum Circuits Using the Big-Batch Tensor Network Method, *Physical Review Letters* **128**, 030501 (2022).
- [29] F. Pan, K. Chen, and P. Zhang, Solving the Sampling Problem of the Sycamore Quantum Circuits, *Physical Review Letters* **129**, 090502 (2022).
- [30] F. Pan, H. Gu, L. Kuang, B. Liu, and P. Zhang, Efficient Quantum Circuit Simulation by Tensor Network Methods on Modern GPUs, *ACM Transactions on Quantum Computing* **5**, 1 (2024).
- [31] G. Kalachev, P. Pantelev, and M.-H. Yung, Multi-tensor contraction for xeb verification of quantum circuits

- (2022), [arXiv:2108.05665 \[quant-ph\]](https://arxiv.org/abs/2108.05665).
- [32] N. Shuttly, M. Newman, and B. Villalonga, Efficient near-optimal decoding of the surface code through ensembling, *Phys. Rev. Lett.* **136**, 070603 (2026).
- [33] See supplemental material for: (1) details to construct the differentiable maximum likelihood estimation framework, (2) complexity analysis of the surface code syndrome likelihood tensor network contraction, (3) training details of the optimization process and analysis of the obtained noise parameters.
- [34] H.-J. Liao, J.-G. Liu, L. Wang, and T. Xiang, Differentiable programming tensor networks, *Physical Review X* **9**, 031041 (2019).
- [35] J. Kelly, R. Barends, A. G. Fowler, A. Megrant, E. Jeffrey, T. C. White, D. Sank, J. Y. Mutus, B. Campbell, Y. Chen, *et al.*, State preservation by repetitive error detection in a superconducting quantum circuit, *Nature* **519**, 66 (2015).
- [36] C. Gidney, M. Newman, A. Fowler, and M. Broughton, A fault-tolerant honeycomb memory, *Quantum* **5**, 605 (2021).
- [37] L. Aghababaie Beni, O. Higgott, and N. Shuttly, *Tesseract: A search-based decoder for quantum error correction* (2025), [arXiv:2503.10988 \[quant-ph\]](https://arxiv.org/abs/2503.10988).
- [38] O. Higgott, T. C. Bohdanowicz, A. Kubica, S. T. Flammia, and E. T. Campbell, Improved decoding of circuit noise and fragile boundaries of tailored surface codes, *Phys. Rev. X* **13**, 031007 (2023).
- [39] J. Bausch, A. W. Senior, F. J. H. Heras, *et al.*, Learning high-accuracy error decoding for quantum processors, *Nature* **635**, 834 (2024).
- [40] H. Cao, F. Pan, Y. Wang, and P. Zhang, Generative decoding for quantum error-correcting codes (2025), [arXiv:2503.21374 \[quant-ph\]](https://arxiv.org/abs/2503.21374).
- [41] I. Hesner, B. Hetényi, and J. R. Wootton, Using detector likelihood for benchmarking quantum error correction, *Phys. Rev. A* **111**, 052452 (2025).
- [42] A. W. Senior, T. Edlich, F. J. Heras, L. M. Zhang, O. Higgott, J. S. Spencer, T. Applebaum, S. Blackwell, J. Ledford, A. Žemgulytė, *et al.*, A scalable and real-time neural decoder for topological quantum codes, *arXiv preprint arXiv:2512.07737* (2025).
- [43] K. Zhang, Z. Yi, S. Guo, L. Kong, S. Wang, X. Zhan, T. He, W. Lin, T. Jiang, D. Gao, Y. Zhang, F. Liu, F. Zhang, Z. Ji, F. Chen, and J. Chen, Learning to decode in parallel: Self-coordinating neural network for real-time quantum error correction (2026), [arXiv:2601.09921 \[quant-ph\]](https://arxiv.org/abs/2601.09921).
- [44] <https://github.com/CHY-i/DMLE-QEC>.
- [45] <https://github.com/TensorBFS/OMEInsumContractionOrders.jl>.

Supplementary Material for "Differentiable Maximum Likelihood Noise Estimation for Quantum Error Correction"

Appendix A: Methods

1. Statistical Mapping of Planar Method

In this section, we elucidate the relationship between the syndrome probability $p_{\theta}(\mathbf{s})$ and the partition function \mathcal{Z} of the corresponding spin glass model. The spin coupling is defined as:

$$J_i = (-1)^{e_i} \frac{1}{2} \log \frac{1 - \theta_i}{\theta_i}, \quad (\text{S1})$$

where e_i denotes the i th component of a length- n error configuration $\mathbf{e} \in \{0, 1\}^n$, and θ_i represents the probability of this error component being flipped. The corresponding Hamiltonian for a given \mathbf{e} is expressed as:

$$H_{\mathbf{e}}(\tilde{\mathbf{s}}) = - \sum_{i=1}^n J_i \overleftarrow{\tilde{s}}_i \overrightarrow{\tilde{s}}_i - \frac{1}{2} \log \prod_{i=1}^n \theta_i (1 - \theta_i), \quad (\text{S2})$$

where $\tilde{\mathbf{s}} \in \{\pm 1\}^{n-m+1}$ is the spin configuration, $\overleftarrow{\tilde{s}}_i$ and $\overrightarrow{\tilde{s}}_i$ are two spins adjacent to edge i . The second term serves as a spin-independent constant. We can then derive the probability of a specific error configuration \mathbf{e} as follows:

$$\begin{aligned} & \exp\{-H_{\mathbf{e}}(\mathbf{s} = 1)\} \\ &= \exp\left\{\sum_{i=1}^n (-1)^{e_i} \frac{1}{2} \log \frac{1 - \theta_i}{\theta_i}\right\} \cdot \prod_{i=1}^n [\theta_i (1 - \theta_i)]^{\frac{1}{2}} \\ &= \exp\left\{\frac{1}{2} \log \prod_{i=1}^n \left(\frac{1 - \theta_i}{\theta_i}\right)^{1 - 2e_i}\right\} \cdot \prod_{i=1}^n [\theta_i (1 - \theta_i)]^{\frac{1}{2}} \\ &= \prod_{i=1}^n \left(\frac{1 - \theta_i}{\theta_i}\right)^{\frac{1}{2} - e_i} \cdot [\theta_i (1 - \theta_i)]^{\frac{1}{2}} \\ &= \prod_{i=1}^n \theta_i^{e_i} \cdot (1 - \theta_i)^{1 - e_i} \\ &= p_{\theta}(\mathbf{e}). \end{aligned} \quad (\text{S3})$$

Consider the scenario where a spin is flipped, as illustrated in Fig. S1; this operation changes the signs of the corresponding terms in the Hamiltonian Eq. (S2). This transformation is equivalent to redefining the Hamiltonian using a new error configuration \mathbf{e}' , which is obtained by applying an operator corresponding to the flipped spin onto the original error configuration \mathbf{e} .

One can verify that this new error configuration will also trigger the same set of detectors (e.g., the two red detectors in Fig. S1). This conclusion holds generally for any sequence of spin flips. Consequently, the total probability of observed detector events is proportional to

the partition function of this Ising model:

$$p_{\theta}(\mathbf{s}) = \frac{1}{2} \sum_{\tilde{\mathbf{s}}} \exp\{-H_{\mathbf{e}(\mathbf{s})}(\tilde{\mathbf{s}})\}, \quad (\text{S4})$$

where $\mathbf{e}(\mathbf{s})$ is a reference error configuration consistent with \mathbf{s} . The factor $\frac{1}{2}$ arises because the introduction of the auxiliary spins endows the system with a Z_2 symmetry, which leads to the double-counting of all possible error configurations. As a result, the Kac-Ward formula can be employed to calculate this partition function exactly.

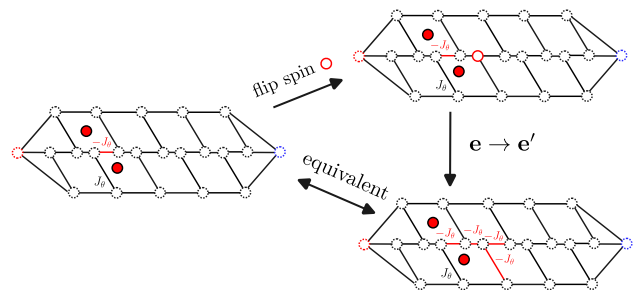


FIG. S1. Equivalent transformation of Ising model.

Here we use a toy model to validate the ability of our gradient-based optimization to recover the underlying prior parameters from simulation data using a $d = 3$ and $r = 5$ repetition code under depolarizing circuit-level noise with error rate $\epsilon_p = 0.001$. This benchmark model, generated from Stim, comprises 12 detectors and 4096 total detector configurations. The manageable system size allows for the direct computation of the complete probability table $p_{\text{data}}(\mathbf{s})$, yielding the exact negative log-likelihood (NLL) loss function. Consequently, we can optimize the parameters θ to recover the prior probabilities with near-exact precision, as shown in Fig. S2. The parameters were initialized as indicated by the orange dashed line. We then calculated $p_{\text{data}}(\mathbf{s})$ for each detector configuration \mathbf{s} using the true prior probabilities and iteratively updated θ until the loss function converged. The gray gradient lines illustrate the evolution of parameters during training. Finally, the parameters converged to the red dots, which exhibit excellent agreement with the true prior probabilities (black line). The inset illustrates the training dynamics, showing the monotonic decrease of the average relative error between the optimized and true priors until convergence. This result demonstrates that, for small-scale models, gradient descent effectively optimizes parameters to near-exact values.

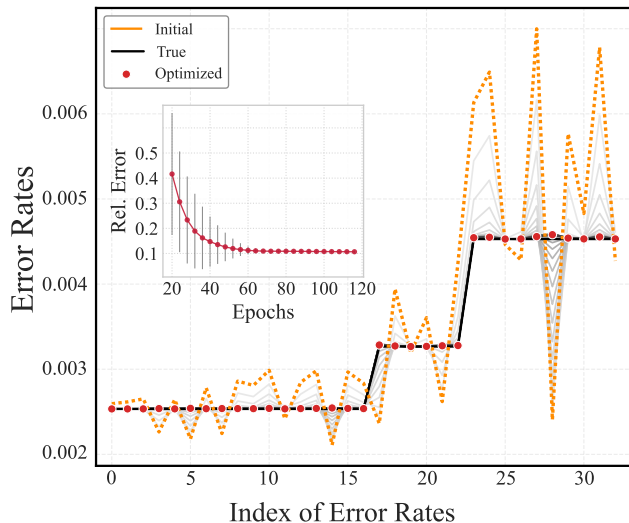


FIG. S2. Benchmark on a $d = 3$, $r = 5$ repetition code. This model contains 12 detectors and 4096 detector configurations. For every configuration \mathbf{s} , we employed the *Planar* algorithm to exactly compute the probabilities $p_{\text{data}}(\mathbf{s})$ and $p_{\theta}(\mathbf{s})$, yielding an exact NLL loss. The orange line represents the initial random perturbative values. The gray gradient lines illustrate the evolution of parameters during training. The red dots and black line represent converged results and the ground truth values.

2. Tensor Network

The aforementioned approach, grounded in the mapping to statistical physics, fundamentally entails identifying a reference error configuration consistent with \mathbf{s} , applying operators that leave \mathbf{s} invariant, and summing over this set of operators. This framework is referred to in the literature as the generator picture [24]. In the context of circuit-level noise, although it is theoretically possible to formulate a tensor network within the generator picture, a significant challenge arises: for complex systems such as the surface code, constructing dual variables for the detectors while maintaining a sufficiently low average degree—a prerequisite for efficient contraction—remains a non-trivial task.

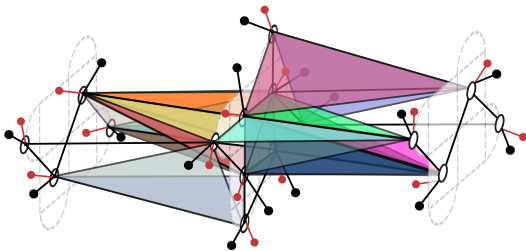


FIG. S3. Tensor network representation of the detector error model for a surface code, constructed in the detector picture. Each XOR tensor enforces detector parity, and probability tensors encode the error mechanism weights.

To address this problem, we directly consider summing over all possible error configurations and setting the probabilities of those configurations that do not satisfy the constraints to zero:

$$p_{\theta}(\mathbf{s}) = \sum_{\mathbf{e}} p(\mathbf{e}) \cdot \delta_{\mathbf{s}, \mathbf{s}_{\mathbf{e}}} . \quad (\text{S5})$$

Further, we can write both \mathbf{e} and \mathbf{s} from the above equation in terms of their components:

$$\begin{aligned} \sum_{\mathbf{e}} p(\mathbf{e}) \cdot \delta_{\mathbf{s}, \mathbf{s}_{\mathbf{e}}} &= \sum_{\{e_i\}} \prod_{i=1}^n \theta^{e_i} (1 - \theta)^{1 - e_i} \prod_{j=1}^m s_j \oplus e_{\partial j} \\ &= \sum_{\{e_i\}} \prod_{i=1}^n P_{e_i} \prod_{j=1}^m X_{e_{\partial j}, s_j} \end{aligned} \quad (\text{S6})$$

where P_{e_i} denotes the probability tensor with components $P_0 = 1 - \theta_i$ and $P_1 = \theta_i$. By introducing a copy tensor for each variable e_i , the probability tensor effectively acts as a weighted copy tensor possessing two non-zero elements, $1 - \theta_i$ and θ_i . Additionally, $X_{e_{\partial j}, s_j}$ is the XOR tensor as defined in main text. This class of tensor network representations is known as the detector picture [24].

Furthermore, in practical implementations, certain XOR tensors exhibit an excessively large degree, causing the tensor network to exceed the memory capacity of a single GPU during initialization. To address this, we utilize the Walsh-Hadamard transform to decompose a high-degree XOR tensor into a central summation index conjugated by Hadamard matrices on each leg [24].

$$X_{ijk\dots} \propto \sum_{\alpha} H_{ai} H_{aj} H_{ak} \dots \quad (\text{S7})$$

This factorization significantly reduces memory overhead, as only the decomposed components need to be stored.

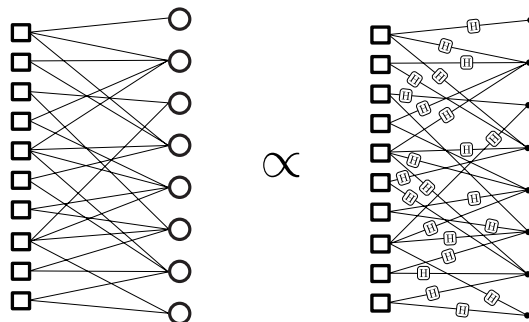


FIG. S4. Walsh-Hadamard transform. The left and right sides respectively show the tensor network structures before and after transformation.

Another major advantage of this factorization scheme is that the tensor networks used for both decoding and optimization share an identical structure, differing only

in the values of specific tensor elements. For a single logical qubit, maximum likelihood decoding requires comparing $p(l = 0)$ and $p(l = 1)$, which is equivalent to computing the sign of the difference, $p(l = 0) - p(l = 1)$. Calculating this quantity allows us to easily decompose the high-degree XOR tensor associated with the logical operator into a set of vectors. Once these vectors are absorbed into the probability tensors, they merely flip the signs of the tensor elements [24]. We present a brief proof below. Assuming the XOR tensor has been factorized, the contraction of the entire tensor network can be rewritten in the following form:

$$\sum_i A_i H_{il} = p_l, \quad (\text{S8})$$

where the two elements of p_l represent the probabilities $p(l = 0)$ and $p(l = 1)$, the H_{il} denotes the final Hadamard tensor connected to logical check vector, and A_i represents the contraction result of the remainder of TN. Utilizing the unitary property of the Hadamard tensor, we can deduce that:

$$A_1 \propto p_0 - p_1. \quad (\text{S9})$$

Fundamentally, the decoding problem reduces to evaluating A_1 . Moreover, it is straightforward to see that the index i corresponds directly to the summation index in Eq. (S7). While this index is set to 1, all connected Hadamard tensors reduce to vectors and can be absorbed into the probability tensors. This absorption process effectively only flips the signs of specific elements (i.e., $\theta \rightarrow -\theta$) within the probability tensors. Consequently, for a given system, we only need to determine an efficient contraction path for a single tensor network structure, which significantly reduces our computational overhead.

Appendix B: Complexity Analysis

By applying the Walsh-Hadamard transformation, we decompose all XOR tensors into Hadamard matrices and copy tensors, with the latter represented using hyper-indices. This leaves only two types of components in the tensor network: one-dimensional error probability vectors and Hadamard matrices, dramatically simplifying the network structure underlying our differentiable maximum likelihood estimation method. We then employ the tensor network contraction path finder from our previous work [28–30], specifically the OMEInsumContractionOrders.jl [45] implementation, to determine an efficient contraction order. The path finder utilizes the combination of both time complexity, memory cost and memory access cost as the loss function, utilizes contraction tree simulated annealing to find the optimal contraction order [31]. The resulting contraction complexity for the $d=5$ rotated surface code with rounds ranging from 5 to 25 is plotted in Fig. S5.

In contrast to the previous estimate that tensor network contraction for a $d=5$, $r=25$ rotated surface code would require tens of CPU years using the boundary MPS scheme [5, 32], our simplified tensor network representation combined with a high-performance contraction path finder reduces the complexity drastically—without any tensor compression. The total contraction cost (in FLOPS) for $d=5$, $r=25$ is 6.3×10^{11} , and the largest intermediate tensor occupies approximately 1 GB of memory. On a high-end NVIDIA H200 GPU, which delivers around 3×10^{13} floating-point operations per second with 144 GB of memory, we can comfortably batch-contract approximately 32 syndromes simultaneously, completing each batch in seconds. This enables both efficient dMLE training and maximum likelihood decoding for surface codes at a scale previously considered computationally prohibitive [5, 24, 32].

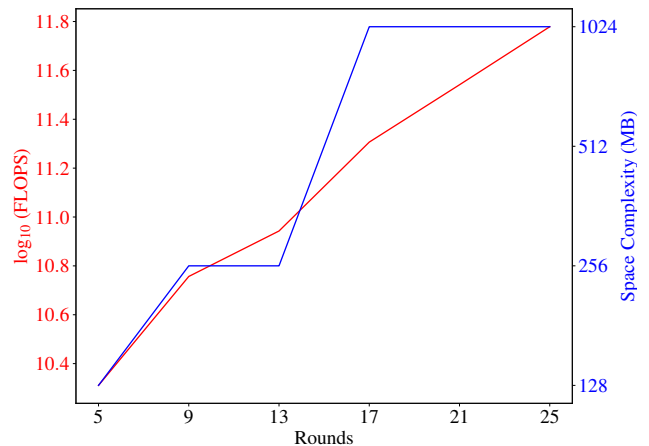


FIG. S5. Contraction complexity of the tensor network for maximum likelihood estimation on the $d=5$ rotated surface code as a function of the number of QEC rounds.

Appendix C: Training Details

The implementation details and hyperparameters for distinct codes are summarized in Tab. S1. For the Repetition (Simulation and BAQIS) and Surface Simulation models, we employed a dataset size of 1,000,000 shots with a batch size of 10,000 and a learning rate of 0.001. In contrast, the Surface Google model was trained with 750,000 shots, a larger batch size of 15,000, and a higher learning rate of 0.01. An error rate of 0.001 was applied exclusively to the simulation-based scenarios. Regarding training duration, the Repetition schemes underwent 500 epochs, whereas the Surface Simulation and Surface Google models required 1,000 and 100 epochs, respectively.

Regarding Google’s experimental dataset, the original dataset comprises 53 subsets, each containing 75,000

samples. Due to limited computational resources, we did not process the entire corpus. Instead, we randomly selected ten representative subsets (indices: 0, 2, 10, 12, 16, 18, 24, 32, 46, and 49) for this study. Although the training was conducted on this partial selection, the results are sufficient to demonstrate the effectiveness of our proposed method. Full-scale validation on the complete dataset is reserved for future work.

TABLE S1. Hyperparameters for Different Numerical Experiments

	Repetition Simulation	Repetition BAQIS	Surface Simulation	Surface Google
Error Rate	0.001	–	0.001	–
Num Shots	1,000,000	1,000,000	1,000,000	750,000
Epochs	500	500	1000	100
Batch Size	10,000	10,000	10,000	15,000
Learning Rate	0.001	0.001	0.001	0.01

To further elucidate the distinct characteristics of the DEMs, Fig. S6 presents a comparative analysis of the DEMs. We specifically contrast the models optimized via Tensor Networks and Reinforcement Learning based on Belief Matching against the baseline derived from correlation analysis. A detailed examination of the specific instance sample_00 ($d = 5$, $r = 9$) reveals a critical distinction in optimization strategies. As shown, the mean error rate of the RL-optimized DEM remains quantitatively proximal to the correlation baseline. Conversely,

the DEM optimized by our proposed method exhibits a substantial deviation. This suggests that the RL approach functions primarily as a local fine-tuning mechanism constrained by the correlation initialization, rather than learning a fundamentally distinct error model. This heavy reliance on the correlation prior offers a plausible explanation for the RL method’s limited generalization capability across different decoders, as observed in our broader experiments.

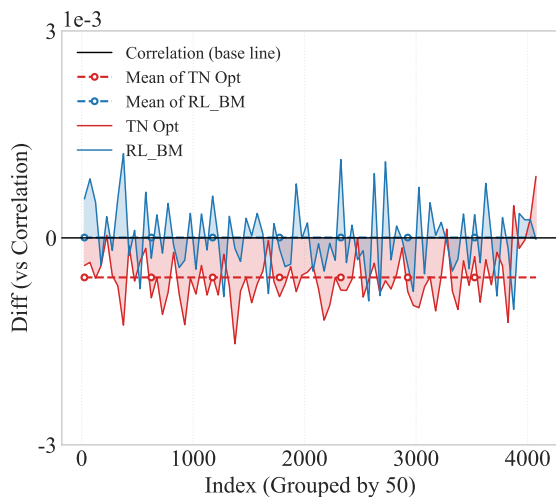


FIG. S6. The differences between DEM optimized via Tensor Network (red), DEM optimized via Reinforcement Learning based on Belief Matching (blue), and DEM obtained through Correlation Analysis.